Article:
Chen, W., Mills, R. and Dwyer-Joyce, R.S. (2015) Direct load monitoring of rolling bearing contacts using ultrasonic time of flight. Proceedings of the Royal Society A: Mathematical, Physical and Engineering Sciences, 471 (2180). 20150103. ISSN: 1364-5021

https://doi.org/10.1098/rspa.2015.0103

Direct Load Monitoring of Rolling Bearing Contacts using Ultrasonic Time of Flight

W Chen, R Mills, R S Dwyer-Joyce

Leonardo Centre for Tribology, Department of Mechanical Engineering, University of Sheffield, Mappin Street, S1 3JD, Sheffield, UK

Abstract

The load applied by each rolling element on a bearing raceway controls friction, wear, and service life. It is possible to infer bearing load from load cells or strain gauges on the shaft or bearing housing. However this is not always simply and uniquely related to the real load transmitted by rolling elements directly to the raceway. Firstly, the load sharing between rolling elements in the raceway is statically indeterminate. And secondly, in a machine with non-steady loading the load path is complex and highly transient being subject to dynamic behavior of the transmission. This study describes a method to measure the load transmitted directly by a rolling element to the raceway by using the time of flight (ToF) of a reflected ultrasonic pulse.

A piezoelectric sensor was permanently bonded onto the bore surface of the inner raceway of a cylindrical roller bearing. The time of flight of an ultrasonic pulse from the sensor to the roller-raceway contact was measured. This depends on the speed of the wave and the thickness of the raceway. The speed of an ultrasonic wave changes with the state of the stress; known as the acoustoelastic effect. The thickness of the material varies when deflection occurs as the contacting surfaces are subjected to load. In addition, the contact stiffness changes the phase of the reflected signal and in simple peak to peak measurement, this appears as a change in the ToF. In this work the Hilbert transform was used to remove this contact dependent phase shift.

Experiments have been performed on both a model line contact and a single row cylindrical roller bearing from the planet gear of a wind turbine epicyclic gearbox. The change in ToF under different bearing loads was recorded and used to determine the deflection of the raceway. This was then related to the bearing load using a simple elastic contact model. Measured load from the ultrasonic reflection was compared with the applied bearing load with good agreement. The technique shows promise as an effective method for load monitoring in real bearing applications.

Keywords: *Load monitoring, Rolling bearing contacts, Piezoelectric sensor, Time of flight, Acoustoelastic effect, Ultrasonic reflection*

1. Introduction

Rolling bearings are key components in rotating machines, and bearing failure is a major cause of the breakdown in the machines. Bearing failures can be catastrophic and result in increasing downtime and maintenance cost, especially for those applications with limited accessibility. Knowledge of load is essential information for the design and the prediction of bearing service life. Rolling bearing life is commonly evaluated by the classical standard ISO 281 [1] in the design stage and this works effectively for most bearings in general applications. However, for those applications with highly fluctuating and dynamic load, like wind turbines, there are unexpected premature failures during the operation [2]. The bearing failure in the gearbox is reported to be responsible for up to one-third of wind turbine failures, which significantly reduce the wind turbine availability [3].

To properly predict bearing fatigue life, accurate load and load history data is needed. Bearing load can be measured directly with load cells or strain gauges on the bearing housing or the shaft [4, 5]. A disadvantage of these techniques is these devices handle the bearing as a whole. Consequently the load dynamically transmitted by the rolling element to the race is not characterized. In rolling element bearings the load is shared by a number of rolling element and raceway contacts and the exact load in these contacts cannot always be uniquely derived from the load on the shaft or bearing. In some machines it may difficult to determine the bearing load, particularly where the load paths are complex and/or highly transient. For instance, load on the bearing in wind turbines is not easily derived from load on the blades or the shaft where it is measured due to complex load paths and the nature of highly varying loading.

In this paper, a novel approach has been investigated in which the load transmitted at rolling contacts is deduced from measurement of ultrasonic reflection. The ultrasonic technique has been widely used in non-destructive condition monitoring and recently in tribological applications. It has been successfully used for investigation of contact between rough surfaces [6] and oil film thickness measurement both in hydrodynamic and elastohydrodynamic lubrication [7, 8, 9]. This study seeks to measure load in rolling contacts by measuring the change in time of flight (ToF) of the ultrasonic wave reflected at the contact interface. The ToF of the reflected pulse is governed by the speed of wave and the thickness of the raceway. The ultrasound speed varies with the state of the stress (acoustoelastic effect) and the thickness of the raceway varies with applied load (deformation). As a consequence, the change in ToF is directly related to load in contact. In this paper ToF measurements have been recorded from both a model line contact and rolling bearing contact, and a method is developed to deduce contact load from the recorded data.

2. Time of Flight of Reflected Ultrasound From A Rolling Contact Interface

Figure 1 shows typical longitudinal ultrasonic waveforms reflected from the back surface of a raceway when (a) it is free and unloaded, and (b) it is loaded by a rolling element. The

ultrasonic transducer is directly coupled to the raceway and so the first pulse received by the sensor is the reflection from the front face of the raceway (transducer - raceway interface), followed by the first reflected pulse from the back face of the raceway (i.e. contact interface in unloaded and loaded state). As the wave reverberates in the raceway, the ultrasound undergoes a series of subsequent reflections received by the transducer. This is illustrated by peaks B and C, the 2nd reflection and the 3rd reflections from the back face of the raceway, respectively. The time interval between adjacent peaks (ToF_0 or ToF_P) is governed by the wave path length ($2d_0$ or $2d_P$) and the wave speed of in the material (c_0 or c_P). As the raceway is loaded by the passage of the rolling element, the wave path length reduces ($2d_P < 2d_0$). Also, the speed of the ultrasound in the stressed material increases ($c_P > c_0$) and therefore the time of flight reduces ($ToF_P < ToF_0$). With the wave propagation energy will be lost due to transmission at the interface (which is much greater in the loaded case), wave dispersion and attenuation in the raceway. Therefore, the amplitude of the signal reduces with the wave path.

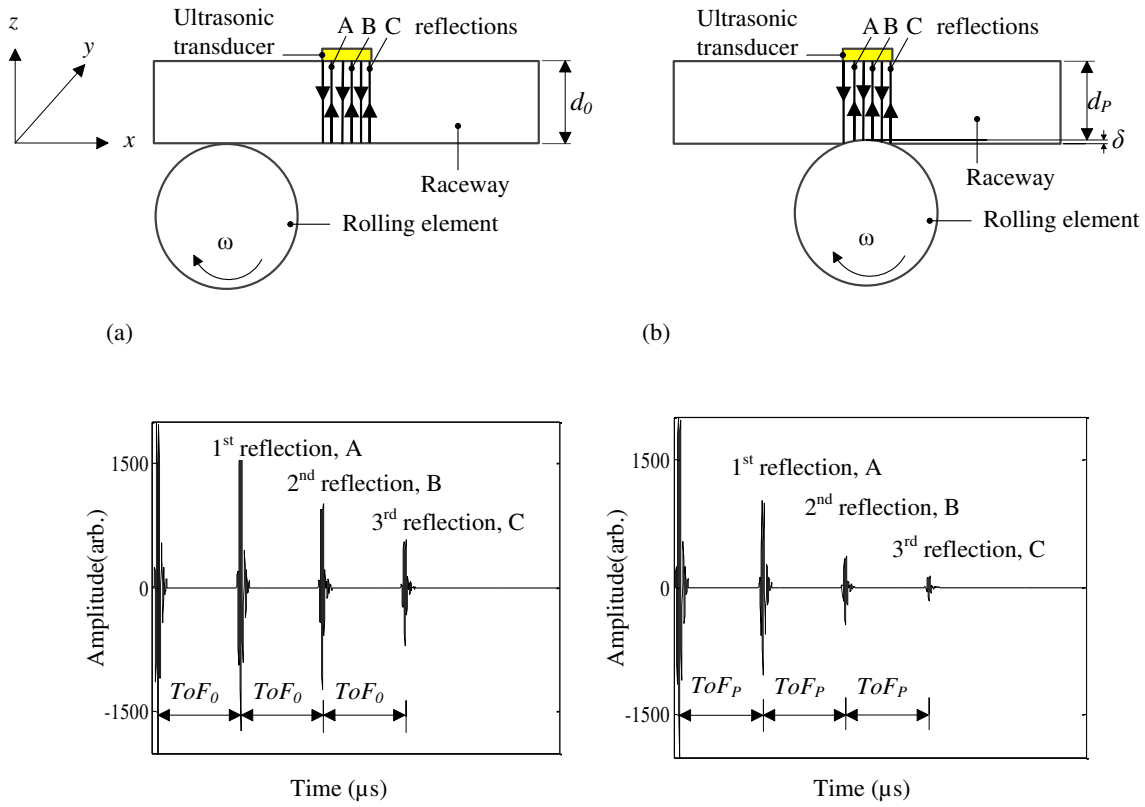

Figure 1.Typical ultrasonic waveform from (a) an unloaded raceway and (b) a loaded raceway-roller contact. The waveform consists of the reflection from the front face of the raceway and subsequent reverberations from the contact surface of the raceway (A, B, and C).

2.1 Time of Flight Change by Deflection

The time of flight is determined by the wave path and the speed of ultrasound in the material:

$$ToF_0 = \frac{2d_0}{(c_{zz})_0} \tag{1}$$

where d_0 is the thickness of the unloaded raceway, $(c_{zz})_0$ is the wave speed in the unloaded raceway in the z direction. When the raceway is loaded by the passage of a rolling element, deflection causes the wave path length to change from $2d_0$ to $2d_P$ as shown in figure 1 (the oil layer is very small compared to the surface distortion, and can be neglected), then the ToF under load becomes:

$$ToF_P = \frac{2d_P}{(c_{zz})_P} \tag{2}$$

If the contact deformation in the raceway denoted by δ, and then the ultrasonic wave path reduces by $2d_P = 2d_0 - 2\delta$. The contribution to time of flight change by geometrical deformation alone that is if $(c_{zz})_P = (c_{zz})_0$, is then given by:

$$\Delta t_\delta = ToF_0 - ToF_P = \frac{2\delta}{(c_{zz})_P} \tag{3}$$

2.2.Time of Flight Change by the Acoustoelastic Effect

2.2.1 Acoustoelastic Effect

The speed of ultrasonic wave in a material depends on the state of the stress; this is known as the acoustoelastic effect [10]. A wave exhibits most sensitivity to stress when the particle motion and the stress field share the same direction [11]. Therefore, a longitudinal wave from an ultrasonic transducer propagating through a raceway will be strongly affected by the high normal stress field. The speed of the longitudinal wave $(c_{zz})_P$, in the z-direction in the stressed material can be related to the strain, $(\epsilon_z)_P$ in this direction, given by [10]:

$$\rho_0 (c_{zz})_P^2 = \lambda + 2\mu + \left[4(\lambda + 2\mu) + 2(\mu + 2m) + 2\nu\mu\left(1 + \frac{2l}{\lambda}\right)\right](\epsilon_z)_P \tag{4}$$

where ρ_0 is the density when the material is unloaded, ν is the Poisson's ratio, λ, μ are second order elastic constants, and l, m are the third order elastic constants. Second order elastic constant and Poisson's ratio are given by:

$$\lambda = \frac{3B(3B - E)}{9B - E} \tag{5}$$

$$\mu = \frac{3BE}{9B - E} \tag{6}$$

$$\nu = \frac{\lambda}{2(\lambda + \mu)} \tag{7}$$

where B is the bulk modulus and E is the elastic modulus of the material. If the wave speed in z-direction in the unstrained state is denoted by $(c_{zz})_0$, then:

$$\rho_0 (c_{zz})_0^2 = \lambda + 2\mu \tag{8}$$

By differentiating equation (4), the relationship between the wave speed and the strain can be written as:

$$\rho_0 (c_{zz})_P \, \mathrm{d}(c_{zz})_P = \left[2(\lambda + 2\mu) + (\mu + 2m) + \nu\mu \left(1 + \frac{2l}{\lambda} \right) \right] \mathrm{d}(\epsilon_z)_P \tag{9}$$

Provided the speed change is small:

$$\rho_0 (c_{zz})_P (c_{zz})_0 \approx \rho_0 (c_{zz})_0^2 = \lambda + 2\mu \tag{10}$$

then the relative change in the wave speed is related to the strain by dividing equations (9) and (10):

$$\mathrm{d}(c_{zz})_P / (c_{zz})_0 = \left[2 + \frac{(\mu + 2m) + \nu\mu \left(1 + \frac{2l}{\lambda} \right)}{\lambda + 2\mu} \right] \mathrm{d}(\epsilon_z)_P \tag{11}$$

By rearranging equation (11), the right side of equation becomes a constant depends on material properties alone.

$$\frac{\mathrm{d}(c_{zz})_P / (c_{zz})_0}{\mathrm{d}(\epsilon_z)_P} = L_{zz} \tag{12}$$

Where L_{zz}, is known as the acoustoelastic constant, and is given by:

$$L_{zz} = 2 + \frac{(\mu + 2m) + \nu\mu \left(1 + \frac{2l}{\lambda} \right)}{\lambda + 2\mu} \tag{13}$$

Based on equations (4-13), the relative change in the wave speed can be predicted according to the strain if the elastic properties of the material are known. The bulk modulus and elasticity modulus of the material are commonly available. However, third order elastic constants are usually obtained by experiments [10, 12, 13]. In this work acoustoelastic constant L_{zz} for bearing steel was determined by experiment to be L_{zz} = - 2.24(see Appendix).

2.2.2 Time of Flight Change by the Acoustoelastic Effect

The strain in the normal direction ϵ_z is not constant but varies from a maximum at the contact surface reducing with depth through the component. The ultrasonic speed in the normal direction will therefore also vary through the component depth. The cumulative effect of the varying strain field must be used to determine the change in the ultrasonic wave speed and hence ToF change. For the case of varying strain through the component thickness d_P, the average strain can be expressed as:

$$\bar{(\epsilon_z)}_P = \frac{\int_0^{d_P} (\epsilon_z)_P \, \mathrm{d}z}{d_P} \tag{14}$$

The ultrasonic speed change between different load cases can be obtained from the strain change in the material once the acoustoelastic constant for the material is known, and equation (12) becomes:

$$\Delta c_{zz} = L_{zz} (c_{zz})_0 \, \Delta\epsilon_z \tag{15}$$

where $\Delta c_{zz} = (c_{zz})_0 - (c_{zz})_P$ and $\Delta\epsilon_z = - (\epsilon_z)_P$. Then the wave speed in z-direction under applied load can be obtained from:

$$(c_{zz})_P = (c_{zz})_0 (1 - L_{zz}\Delta\epsilon_z) \tag{16}$$

The time of flight change due to the acoustoelastic effect alone (i. e. caused only by the ultrasonic speed change) is given by:

$$\Delta t_c = \frac{2d_0}{(c_{zz})_0} - \frac{2d_0}{(c_{zz})_P} \tag{17}$$

Substituting equation (16) into equation (17) gives:

$$\Delta t_c = \frac{2d_0}{(c_{zz})_0} \left(\frac{-L_{zz}\Delta\epsilon_z}{1 - L_{zz}\Delta\epsilon_z} \right) \tag{18}$$

As the deformation in the contacting surface is defined by strain:

$$\delta = \Delta\epsilon_z d_0 \tag{19}$$

Then the equation (18) becomes:

$$\Delta t_c = \frac{-2d_0 L_{zz}\delta}{(c_{zz})_0 (d_0 - L_{zz}\delta)} \tag{20}$$

2.3.Apparent Time of Flight Change by the Phase Change

The easiest practical way to determine the ToF of ultrasound is to measure the time between the relevant reflection peaks in the waveform using a zero-crossing method (as shown in figure 2a). For the case of ultrasonic reflection from a free surface (i.e. a surface that is not in contact with another component) the boundary does not affect the phase of the reflected wave and a zero-crossing method can be used to measure the ToF. This method is commonly used, for example to determine the tension in a threaded fastener from the change in ToF under load. There is no phase shift between the unloaded reference and the loaded signal in figure 2a and the time difference, Δt, between the zero point of the reference signal and the corresponding zero point of the loaded signal, represents the change in ToF of the ultrasound due to the change in the length of the component.

However, for the case of a reflection from a contact with another component, the phase of the reflected wave changes. The magnitude of the phase change (and indeed the signal amplitude) is determined by the contact condition [14]. However, the contact condition cannot be known a-priori as the bearing lubrication regime depends on applied load, bearing speed, material properties and the roughness of contact surfaces. The phase change in the signal affects the timing of the zero-crossing points of the reflected wave and so gives inaccurate measurement of ToF.

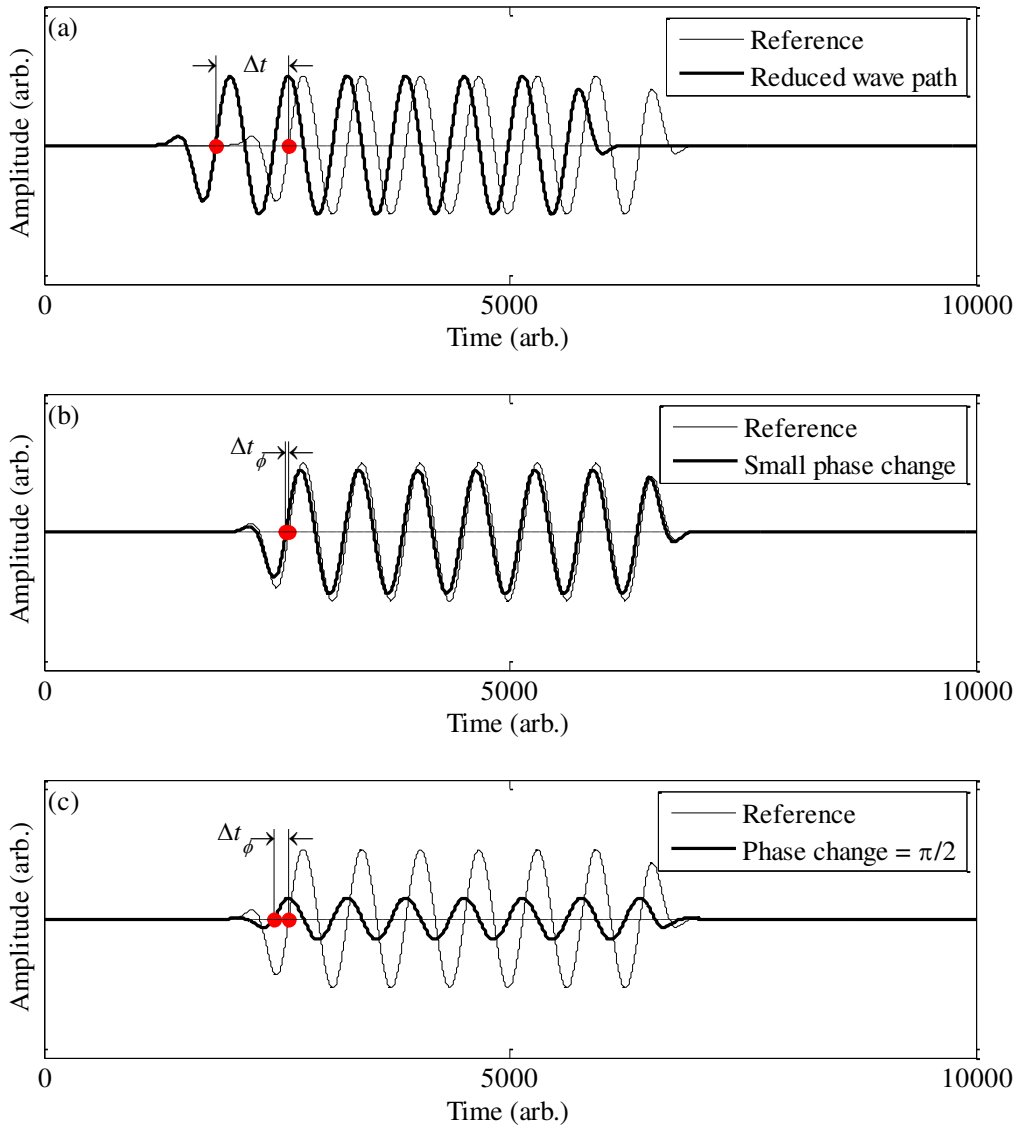

Figure 2. Schematic diagram showing the change in ToF between two ultrasonic signals determined by a zero-crossing approach. The change in ToF between the reference signal and the loaded signal is caused by: (a) a length change of the wave path, (b) a small phase change from a lightly loaded contact and (c) a phase change of π/2 from a heavily loaded contact.

The effect of phase change on altering the zero-crossing points of the reflected wave is schematically in figure 2 (b) and (c). Three ultrasonic signals from a surface in different conditions are shown. The reference is a reflected signal from a surface in unloaded and free (out of contact with other components) state, and the signal with small phase change is reflected from the surface in a lightly loaded mating condition in which a thick oil film layer is formed. The signal with a phase change of π/2 is a reflection from the surface in a heavily loaded mating condition in which the oil film layer becomes vanishingly thin. In the schematic figures 2(b) and 2(c), only the ToF change due to phase shift is shown and it is

assumed that there is no length change in the wave path. The phase change results in an apparent change in the ToF, which is denoted by Δt_ϕ, given by:

$$\Delta t_\phi = \frac{\phi_R}{2\pi f} \tag{21}$$

Where ϕ_R is the phase change between the reference signal (unloaded state) and the reflected signal in loaded state, and f is the centre frequency of the ultrasonic wave. The magnitude of the phase change for different contact cases has been studied by Reddyhoff et al [14] and depends on the stiffness of the interface, K, according to:

$$\phi_R = \arctan \frac{4\pi f K z_1 z_2^2}{K^2\left(z_1^2 - z_2^2\right) + \left(2\pi f z_1 z_2\right)^2} \tag{22}$$

where z_1 and z_2 are the acoustic impedance of the contact media. For a contact separated by a lubricant film of thickness, h, the stiffness of the oil layer is given by [7]:

$$K = \frac{B}{h} \tag{23}$$

where B is the bulk modulus of the lubricant.

As an illustration of the magnitude of the phase effect, if the oil film between steel and steel is 0.5 μm, then the phase change (according to equation (22) and (23)) will be 1.12 radians. When using an ultrasound transducer with nominal central frequency of 10 MHz, the change in ToF from this phase shift effect is 17.8 ns. This is significant compared to ToF change from load and cannot be neglected. Section 3.4 in this paper describes the processing of signals using a Hilbert Transform to remove this phase effect.

2.4.Total Time of Flight Change

The total change in time of flight between reflected ultrasonic waves is thus the summation of the effect of deflection, change in the ultrasonic speed, and phase change according to:

$$\Delta t = \Delta t_\delta + \Delta t_c + \Delta t_\phi \tag{24}$$

where Δt_δ and Δt_c directly depend on load, and Δt_ϕ depends on the contact condition which indirectly depends on load. Substituting equation (3), (20) and (21) into equation (24), then the total time difference between the reflected ultrasonic pulse from a free surface and the reflected pulse from loaded contact surface becomes:

$$\Delta t = \frac{2\left(1 - L_{zz}\right) d_0 \delta}{\left(c_{zz}\right)_0 \left(d_0 - L_{zz}\delta\right)} + \frac{\phi_R}{2\pi f} \tag{25}$$

2.4. Prediction of Change in Time of Flight from a Cylindrical Roller Bearing Contact

By way of an example, the predicted time of flight change from a cylindrical roller bearing contact is calculated. Table 1 shows the bearing geometry and properties. The deflection of the raceway, δ is obtained from the empirical relationship developed by Palmgren [15]:

$$2\delta = 3.84 \times 10^{-8} \frac{P^{0.9}}{\left(l_0 \times 1000\right)^{0.8}} \tag{26}$$

where P is the normal contact load in Newtons and l_0 is the roller effective length in meters.

Table 1 Cylindrical roller bearing geometry and properties

Test bearing outer diameter, m	0.367
Test bearing inner diameter, m	0.259
Roller diameter, m	0.054
Effective roller length, m	0.079
Inner raceway thickness, m	0.0195
Number of rollers	15
Poisson's ratio	0.3
Modulus of Elasticity, GPa	207

The oil film thickness is predicted from the well-known Dowson and Higginson equation [16]. The oil film thickness is used to calculate the stiffness using equation (23) and then the phase change using equation (22). This in turn is used to determine the apparent time of flight change due to phase shift. The deflection from equation (26) is then used in equation (3) and (20) to find the time of flight change contributed by the deflection and the ultrasonic speed change respectively. Figure 3 shows the contribution of the three components as the bearing contact load is increased.

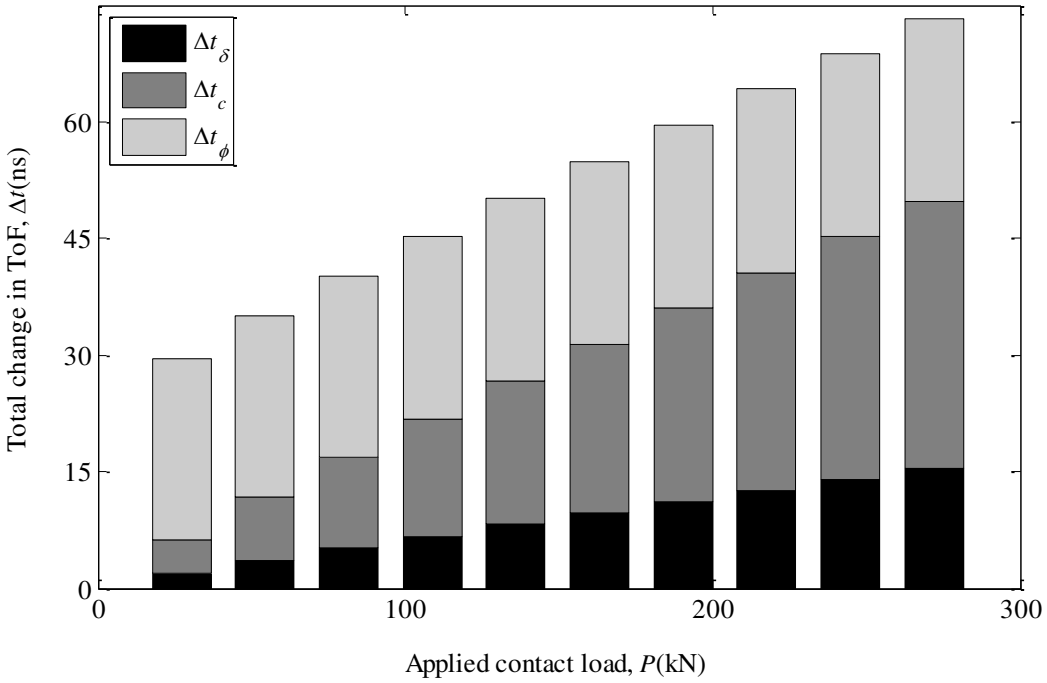

Figure 3. Predicted change in ToF for a rolling bearing contact under various load. For each load, the change in ToF contribution from surface deflection, acoustoelastic effect and phase shift are given.

The change in time of flight of an ultrasonic pulse is small reaching a maximum of ~ 70 ns at the highest bearing contact load. It is clear that all three components are significant and cannot be neglected. At low load, the apparent time of flight change due to the phase change dominates. This remains almost constant as the load increases (the oil film thickness shows comparatively weak dependency on load but a large dependency on speed and lubricant viscosity) whilst the contribution from deflection and change in the ultrasonic speed increase proportionally.

3. Experimental Apparatus

3.1 Model Line Contact Apparatus

Figure 4 schematically shows the model line contact apparatus and instrumentation. Line contacts were formed between cylindrical steel rollers and steel plates under a normal load applied by a hydraulic cylinder. The maximum capacity of the hydraulic cylinder was 100kN. A stepper motor controlled by a LabVIEW routine was used to index the central plate as shown in figure 4. In this way, the top roller could be rolled back and forth beneath the sensor location. An ultrasonic sensor was bonded on the upper plate as shown. A small window on the loading frame allowed for the sensor location and wire connection.

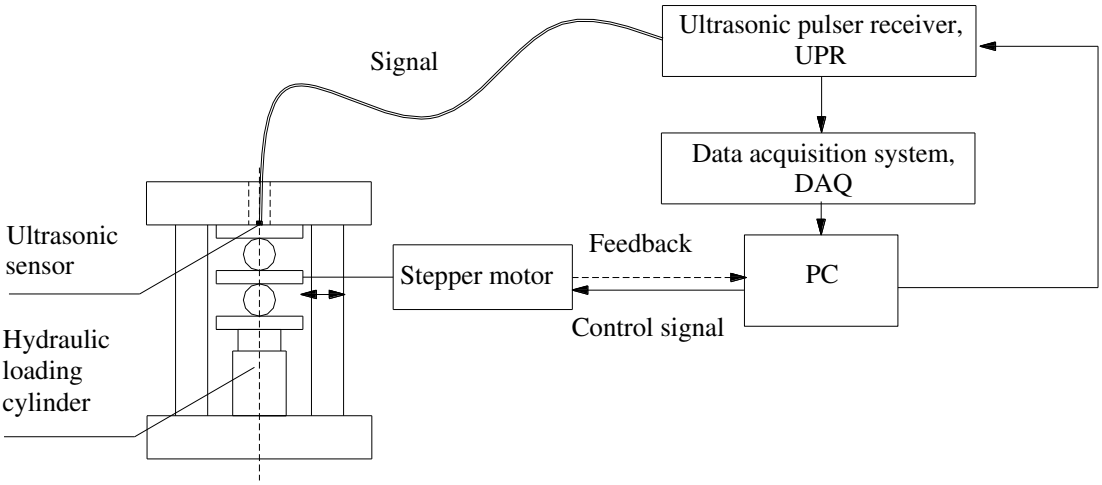

Figure 4. Schematic diagram of the model line contact apparatus and ultrasonic measurement instrumentation.

3.2 Instrumentation

The ultrasonic measurement instrumentation consisted of a piezoelectric transducer, an ultrasonic pulser-receiver (UPR) and a data acquisition system (DAQ). An ultrasonic pulse was generated when the transducer was excited by a short duration voltage signal. The wave propagated from the front face to the back face of the upper plate, partly reflected back at the contact interface and received by the same transducer. The UPR was used to generate short duration voltage pulses and receive reflected signals. A 30V 'top hat' signal of 100 ns duration was employed at a repetition rate of 10k pulses per second. The reflected signal was digitized by the DAQ system and streamed directly to the computer for storage. The received signal was digitized at 100M samples per second and an interpolation technique was performed in the data analysis. The analysis can be performed either in an on-line processing routine or a post-processing routine.

3.3 Transducer Design and Installation

The transducers used in this work were made from low cost, off the shelf piezoelectric elements formed from high sensitivity lead zirconate titanate. Piezoelectric elements (PZT) with a nominal centre frequency of 10 MHz were used as they provide good penetration into the steel together with a clear distinct signal. The original elements were in disc form with diameter of 7.1 mm and thickness of 0.2 mm and came pre-coated with wrap around silver electrodes (see figure 5). The spatial resolution of the measurements depends significantly on the ratio of the sensing area to the contact area. As the contact regions in rolling bearing are comparatively small, to improve the spatial resolution, piezoelectric elements were modified to form narrow strips, 7 mm in length and 1 mm in width. Sensors were mounted on the surface of the specimen using a high temperature adhesive. A layer of the epoxy was placed over the sensor to protect the sensor and partially suppress the sensor ringing.

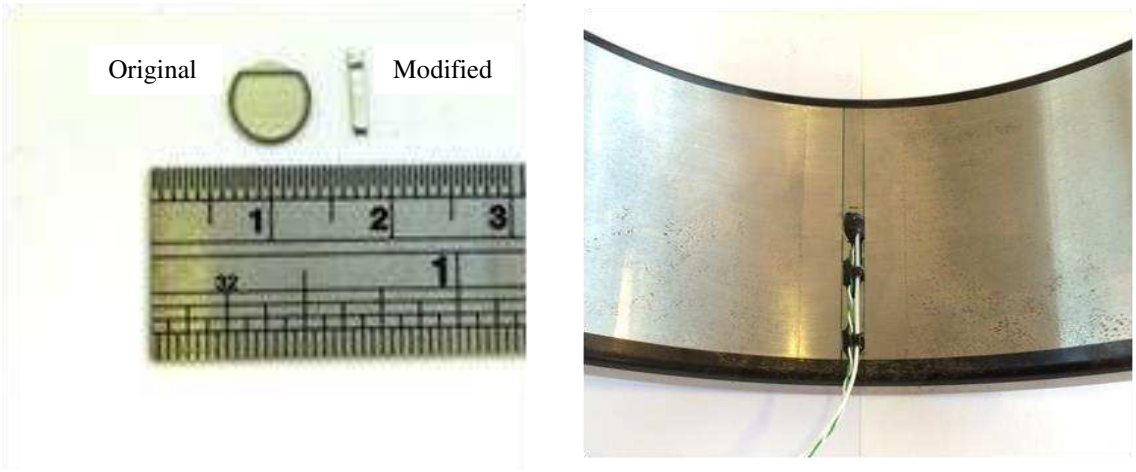

(a) (b)

Figure 5. (a) Photograph of the sensor before and after modification; (b) Modified sensor bonded on the inner race of a roller bearing.

3.4 Signal Processing

The ToF of the ultrasonic wave in the material is the time interval between the first peak (the reflection from the front face) and the second peak (the first reflection from the back face of the specimen) as shown in figure 1. The change in ToF, Δt is the difference in that interval between when the plate is in the unloaded ToF_0, and the loaded state ToF_P. To get the change in ToF, a reference signal for the specimen in the unloaded state is required. The procedure started with recording a reflected signal when the plate was unloaded and this was taken as the reference. The line contact passed through the sensor position at a specific interval and the reflected signal at different positions was recorded. The second peak (peak A in figure 1) was extracted from the waveform.

Figure 6 shows a pair of reflections from contact surface. The reference signal was taken when the plate was unloaded, and the loaded signal was recorded when the loaded plate-roller contact was directly underneath the sensor. The time shift between two signals is clear: the loaded signal is advanced toward to the left compared to the reference signal. This shift is caused by the wave path reducing in length and the increase in the speed of the ultrasonic wave (discussed in section 2.1 and 2.2). But also when the wave reflects at the plate-roller interface it undergoes a phase shift which presents as a time shift to the left of the pulse peaks (discussed in section 2.3). A technique is required to remove the effect of the phase shift.

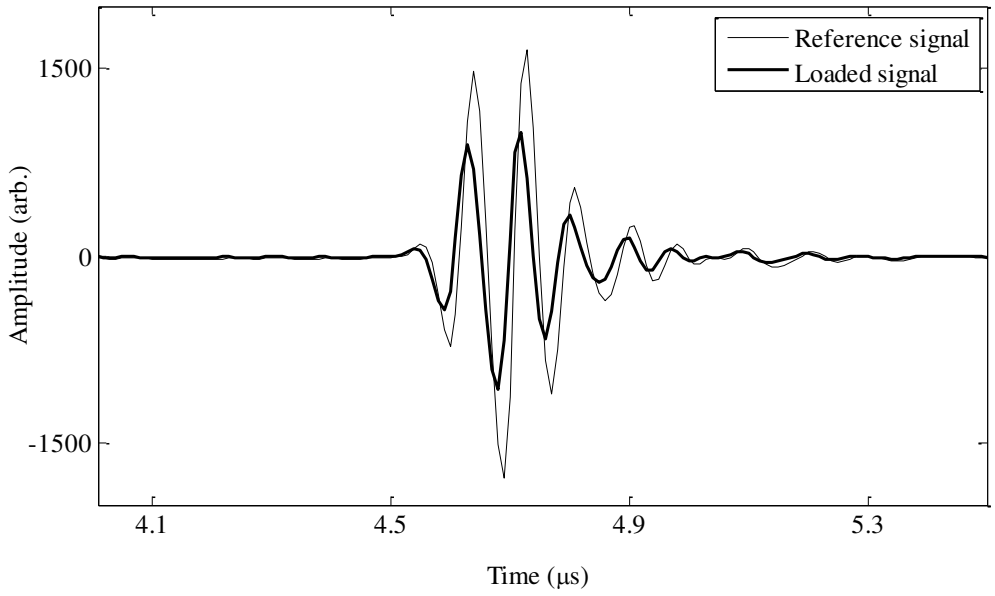

Figure 6. Reflections from the contact face of the upper plate in unloaded and loaded state. Reflection from unloaded plate was taken as a reference.

The Hilbert transform is an operator which takes a real function to produce a convolution of the original function with $1/\pi t$. The Hilbert transform forms an analytic signal from a real signal. An analytic signal is a complex time signal whose real part is the original signal and the imaginary part is the Hilbert transform of the original signal. The signal measured by the ultrasonic transducer is the 'real' component of the ultrasonic wave. The ultrasonic wave however, has an additional 'imaginary' component which can be obtained by applying the Hilbert transform. The result of this process is to obtain the time dependent complex vector of the ultrasonic wave. By calculating the time dependent magnitude of this complex waveform vector, the envelope of the wave, which can be considered analogous to a time based energy profile of the reflected wave, is obtained.

As an example, figure 7 shows the effect of phase shift on the envelopes of the two signals in figure 2c. The reference signal is a simulated reflection from a free surface. The loaded signal is a simulated reflection from the same surface under highly loaded contact having a phase shift approaching $\pi/2$. From the figure, the phase shift between two signals is clear and appears as a modification of the ToF: the solid dark line shifts to the left relative to the reference. Despite the phase change in the reference and the loaded signal, there is no time shift between the Hilbert transform envelopes. It can be also seen that the extent of the two envelopes are independent of the phase of the reflected signal, though the amplitude will vary depending on the proportion of ultrasonic energy which has been transmitted through the contact into the mating component.

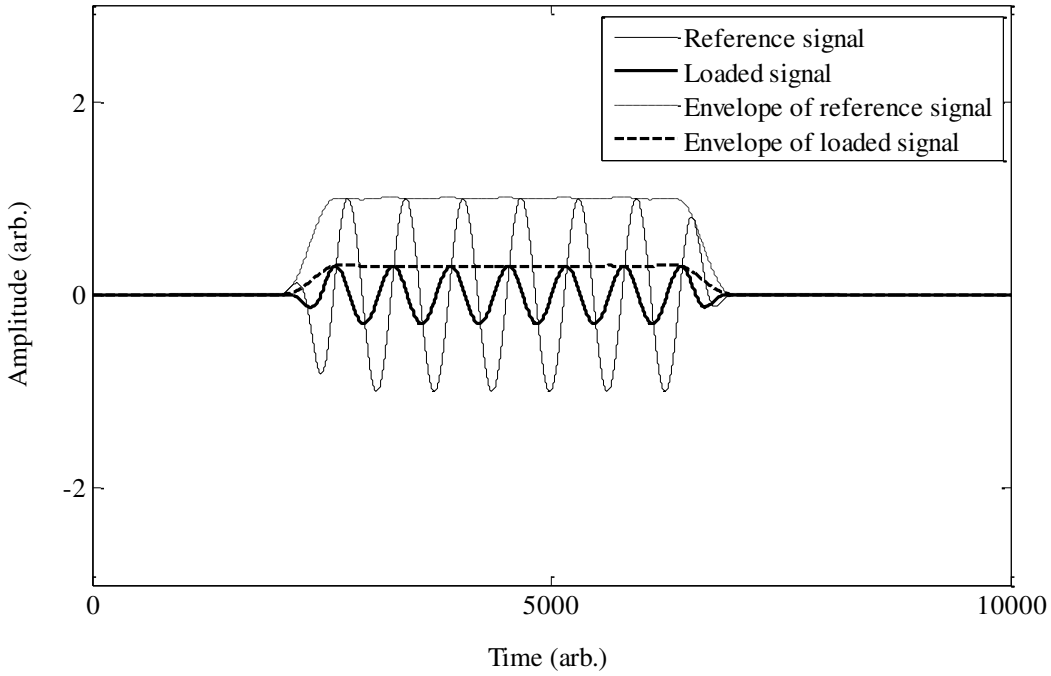

Figure 7. Simulation of phase shift between reference signal and reflected signal. Phase shift between these two signals is evident but there is no phase shift between their envelopes obtained through the Hilbert transform.

By cross correlating the envelope of the reference signal with that of the reflected signal, the time shift of the 'energy packet' of the wave is obtained, corresponding to the change in ToF as a result of geometric deflection and acoustoelastic effects. The time shift of the 'energy packet' is the net change in ToF which excludes the effect of the phase shift. Figure 8 shows the envelopes of the reference and loaded signal from figure 6. The time shift between the envelopes is the change in ToF from the surface deflection and the acoustoelastic effect alone without the effect of the phase shift.

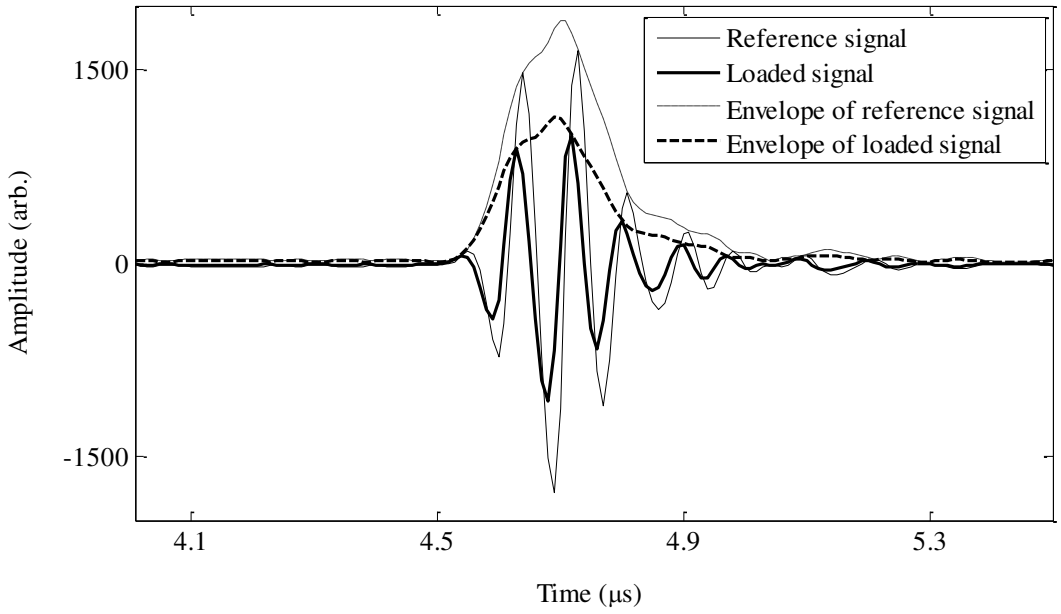

Figure 8. Measured reference signal and loaded signal and their envelopes

The accuracy limitation of this approach is due to the sampling frequency, as the phase shift is measured to the closest sampling point. A simple interpolation was performed on the derivative of the cross correlation of the envelopes to improve the accuracy. For instance, 1/100 of the sampling period precision for measured data was observed, giving an accuracy of 0.1 ns at the sampling frequency of 100 MHz.

4. Experimental Results

As the central plate was driven by the stepper motor, the roller contact approaches the sensor moves underneath it and then recedes. Consequently, the change in ToF increase from zero to a maximum and back to zero again. As an example, figure 9 shows the first reflection from the model line contact in three cases: (a) the contact was away from the sensor location; (b) the contact is below the sensor position; and (c) the contact passed over the sensor location.

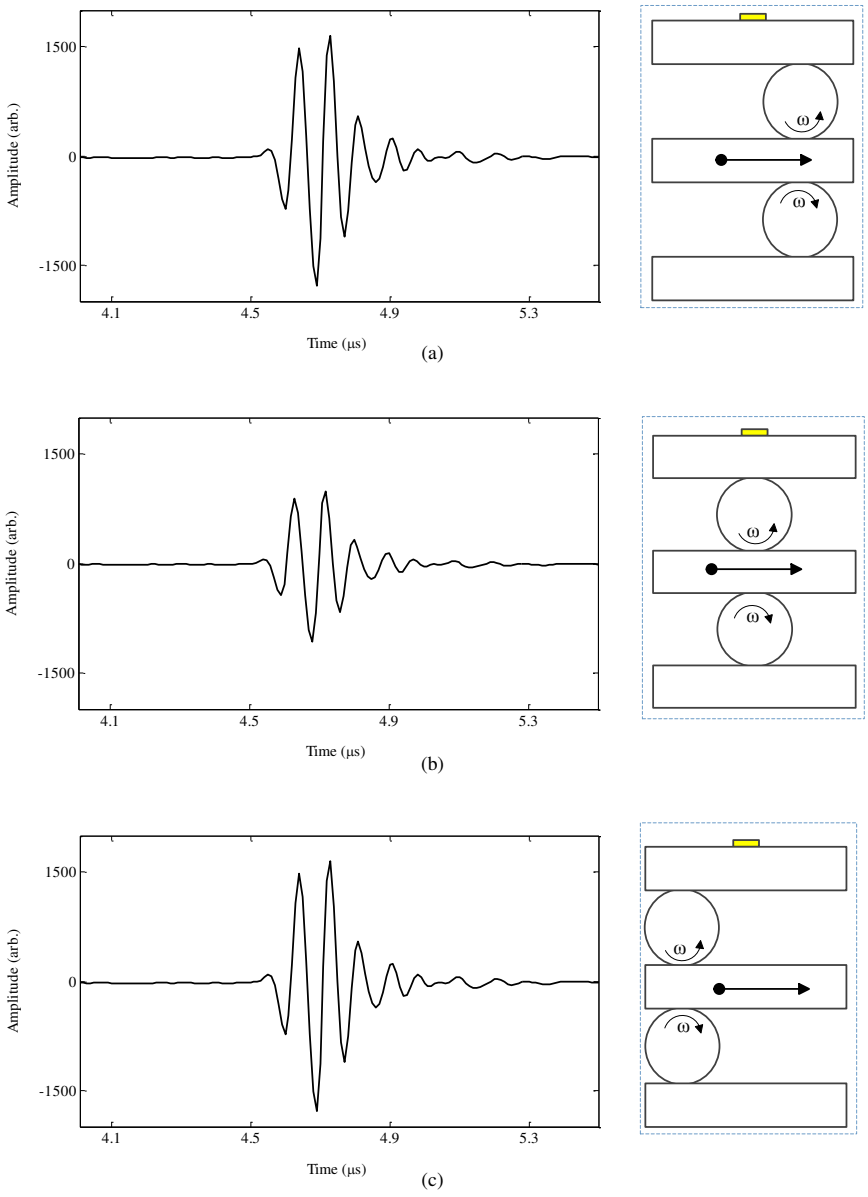

Figure 9. Measured first reflections when the line contact was at different positions under an applied normal load of 26.9 kN.

For each load, the first reflection for various contact positions was recoded. By comparing with the reference signal, the change in ToF can be measured. The magnitude of the change in ToF was obtained by applying cross correlation technique to the envelope of each reflected signal and the envelope of the reference signal. Since the effect of phase shift was excluded from their envelopes, the measured change in ToF was only from applied load.

The predicted change in ToF was calculated by using equations (3), (23) and (26). Using the relationship between load and theoretical prediction of change in ToF, measured change in ToF can be interpreted into measured load. For the model line contact, the comparison between measured contact load and actual applied contact load is given in figure 10.

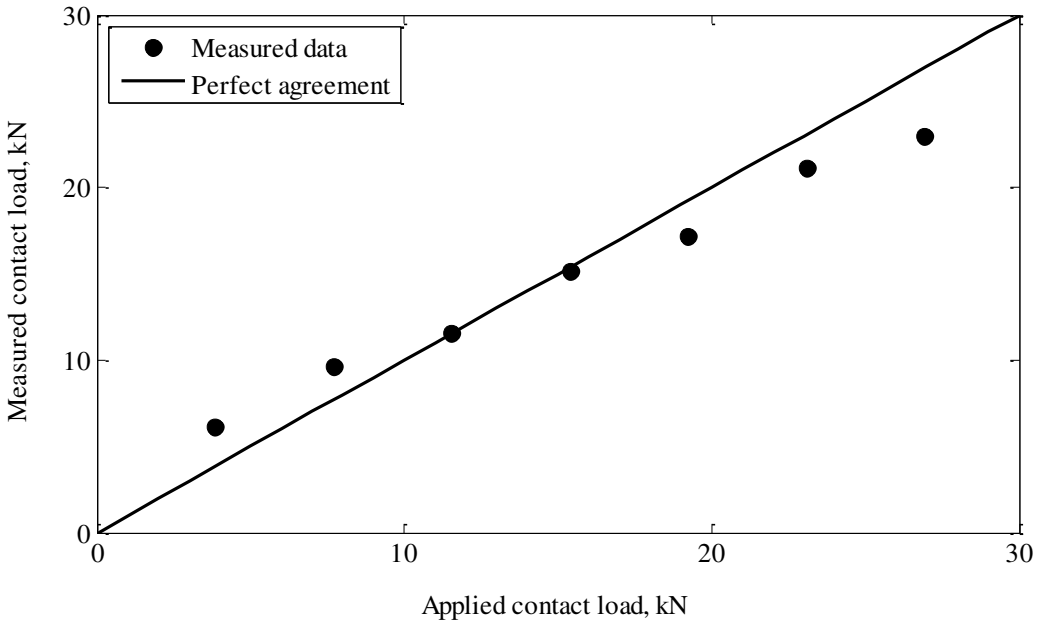

Figure 10. Comparison between measured load from ultrasonic ToF method and applied contact load.

General good agreement is seen between the measured and applied contact load. At lower loads the measured load is slightly over predicted. This is probably caused by the actual contact length being less than the effective length of the roller. The rollers used in the experiment were slightly crowned and so do not form a perfect line contact. This results in a higher contact stress than expected, and so the applied load is over predicted.

5. Application to a Roller Bearing

Ultrasonic load measurements were taken on an NU2244 single row cylindrical roller bearing used in the planetary gear of an epicyclical stage of a 2-megawatt wind turbine gearbox. This bearing was available for test from a pre-existing study [17]. The test rig was driven by a 7.5kW, 1450 rpm electric motor via a pulley-belt system. Figure 11 schematically shows the cylindrical roller bearing rig. The bearing was mounted within a large double row spherical roller bearing, enabling the outer raceway of the test bearing to be rotated at the desired speed. The inner raceway of the test bearing was static, and a radial load was applied to the bearing through a stationary inner shaft via a large hydraulic cylinder with a 1000 kN capacity. The pressure in the hydraulic cylinder was controlled to maintain the desired load on the test bearing. For all load measurements, the test bearing was operated at the speed of 100 rpm.

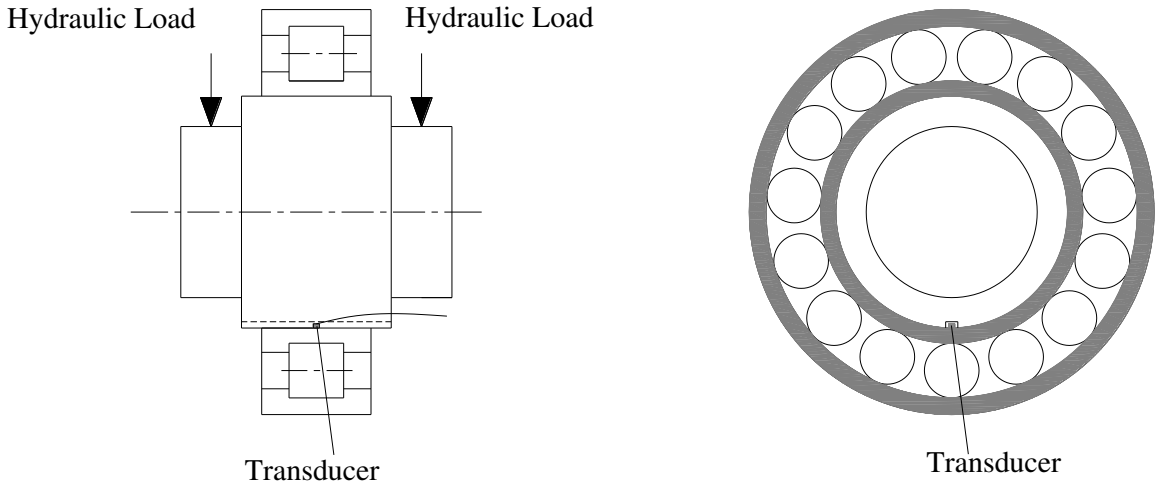

Figure 11. Schematic of the cylindrical roller bearing and transducer location

A modified ultrasonic sensor with central frequency of 10 MHz was permanently bonded to the inner surface of the inner raceway as shown in figure 5b. The inner race was assembled with a stationary shaft on which a slot with width of 5 mm was made for the sensor. The circumferential location of sensor was chosen as shown in figure 11 so that the sensor measured the most highly loaded contact in the bearing. Just as in the model line contact experiment, the sensor received several reflections back from contact interface, but only the first reflection was recorded. When a roller came into contact with the race under the sensor location, the amplitude, phase and arrival time of the signal were modified. The reflections from the contact face in each case have been stacked together and used for data processing. The sampling rate was set to 10 kHz, at this rate approximately 27 reflections were received from each roller passage (note in figure 12b the sampling rate is 1 kHz to clearly show transitions caused by the roller passage).

Figure 12 gives an example of the data obtained from the cylindrical bearing under 980 kN radial load. Figure 12a shows a sequence of contact face reflections for a single complete revolution. A signal window was used to isolate the required reflection from the whole waveform and the isolated part was stored in a first-in-first-out buffer. The first reflections were then sequentially stacked together to form an array. There are 15 significant drops in the amplitude, corresponding to each of the 15 rollers passing under the sensor. A series of data showing the contact before and after passing the sensor position has been extracted and is shown in figure 12b. The amplitude reduced when the contact approached the sensor location, and achieved the minimum value when the contact was directly underneath the sensor. In addition to the amplitude reduction, the time of flight in the inner race also reduced. The contact face reflection from the unloaded race was extracted as reference. A reference signal was compared with a reflected signal from the contact in figure 12c. The time shift is clear; the reflected signal (the thicker line) shifts to the left, which consists of the phase shift from contact interface and the time shift from the compression of the inner race. The contact dependent phase shift was removed from the envelopes by using Hilbert

Transform as described in section 3. The envelope of the reference signal and that of reflected signal from the contact is shown in figure 12d.

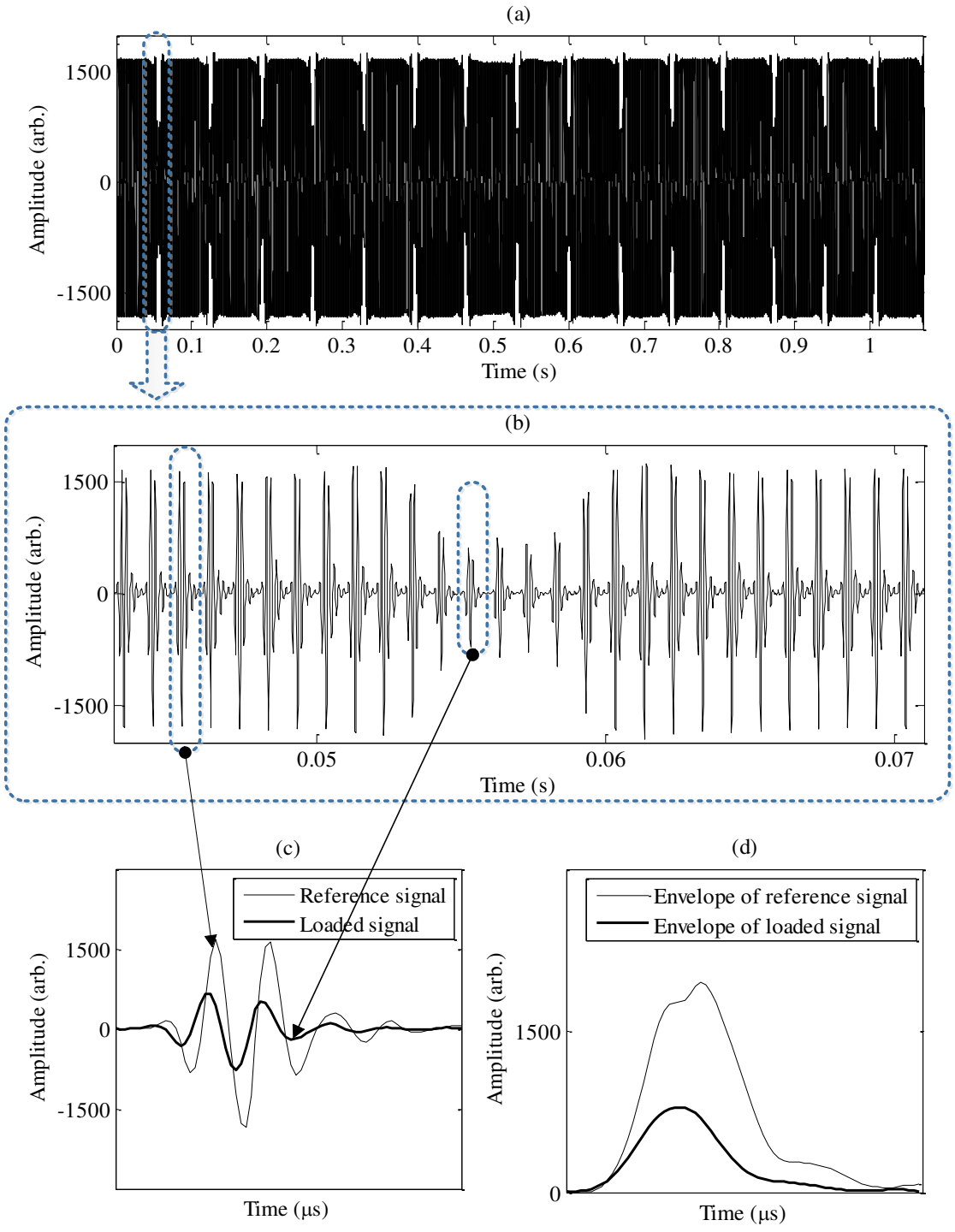

Figure 12. (a) Streamed ultrasonic data for one complete revolution of the bearing under 980 kN radial load; (b) A section of data when a roller passes under the sensor position; (c) Extracted single pulses for contact and out of contact; (d) envelopes of the signal for contact and out of contact.

By cross correlating the envelope of the reference signal with that of the measured signal, the change in ToF as a result of geometric deflection and acoustoelastic effects was obtained.

The change in ToF when rolling contacts pass the sensor location under different bearing loads are shown in figure 13.

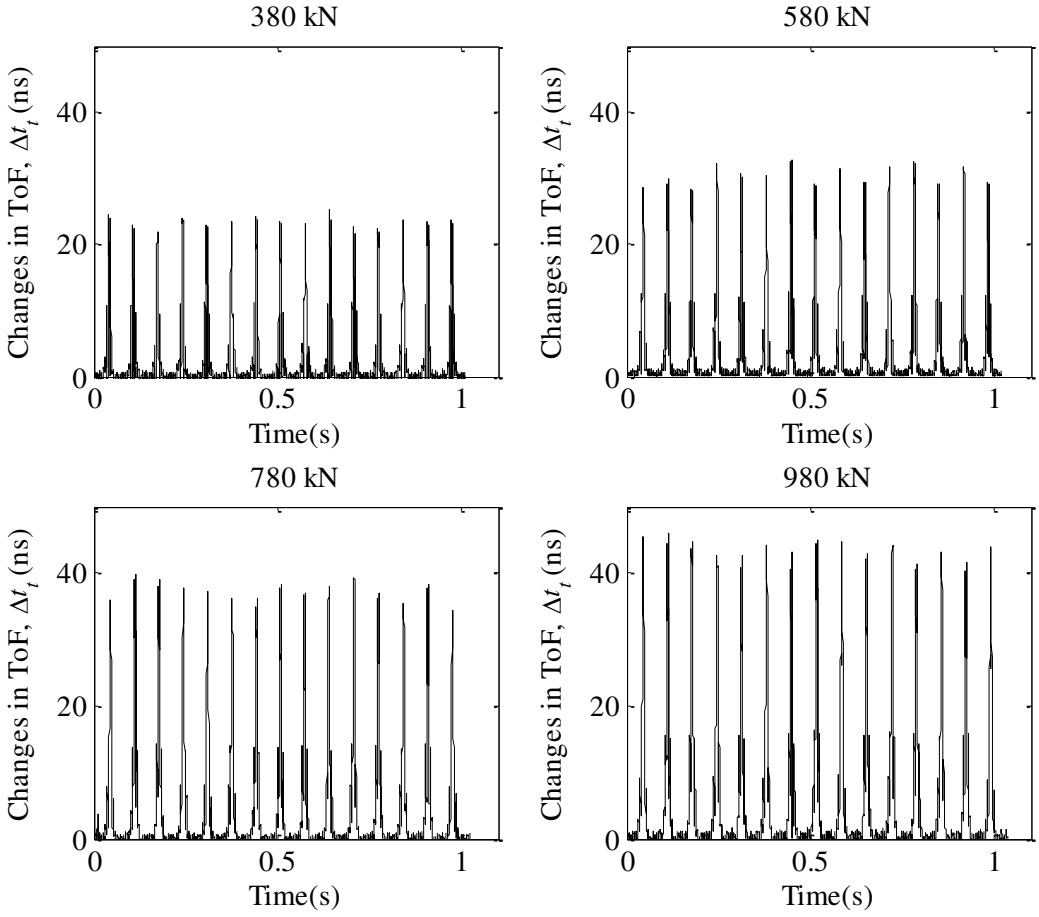

Figure 13. Measured change in ToF for one complete revolution at 100 rpm for the cylindrical bearing under four different loads.

The change in ToF as each rolling contact passes the sensor is clear in figure 13. As the load on the bearing is increased, the ToF increases. The magnitude of change in ToF increased from 22.8 ns to 43.9 ns when the bearing load increased from 380 kN to 980 kN. It can also be observed that the ToF change under a particular load is not exactly the same for each of the 15 rollers, there appears to be a slight periodic variation. At present it is not clear why this should be the case as the roller are all nominally the same geometry and should be subject to the same load as they move into contact. Possibly some slight misalignment of the cage with respect to the raceway may be the cause.

To get the suface deflection of the raceway, the load on the roller-raceway contact is required. The sensor was located at the most loaded zone of the bearing and the maximum load on the roller was calculated by using [18]:

$$P = \frac{4.08W}{N} \tag{27}$$

where W is the normal load on the bearing, N is the number of rollers in the bearing. By combining equation (3), (23) and (26) , the relationship between applied contact load and change in ToF can be expressed as:

$$\Delta t_t = \frac{3.84\times10^{-8}\dfrac{P^{0.9}}{\left(l_0\times1000\right)^{0.8}}\left(1-L_{zz}\right)d_0}{0.5\left(c_{zz}\right)_0\left(2d_0-3.84\times10^{-8}\dfrac{P^{0.9}}{\left(l_0\times1000\right)^{0.8}}L_{zz}\right)} \tag{28}$$

where Δt_t is the change in ToF from the race geometry deflection and the ultrasound speed change.

Using equation (28), the measured change in ToF was converted into contact load. Figure 14 gives a comparison between measured and applied load for the most loaded roller-raceway contact. Good agreement is observed, although as with the data for the model line contact (figure 10), the load is slightly over-predicted at the low end. Again, it is possible roller curvature has a disproportionate effect at low loads.

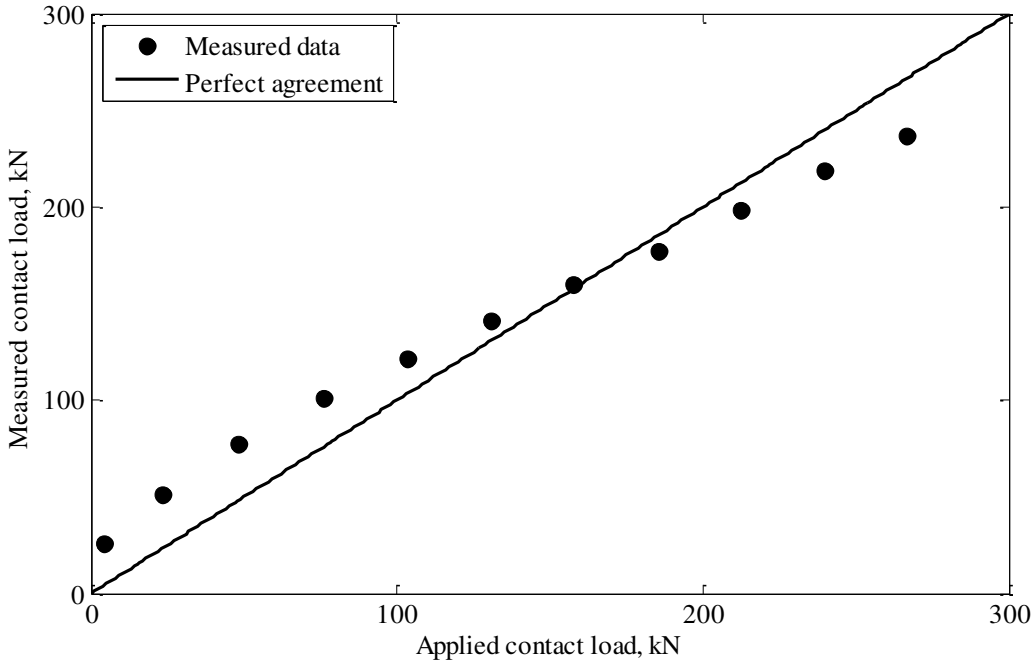

Figure 14. Comparison between measured and applied load in the most loaded roller-raceway contact

6. Conclusion

An ultrasonic time of flight method has been developed to directly measure the load transmitted by a rolling contact. The ToF of a reflected ultrasonic pulse through a contact under varying loads was measured. The change in ToF was the result of elastic deformation of contacting surfaces and the change in wave speed by the acoustoelastic effect. Both of these are directly related to the contact load. A signal processing route using the Hilbert transform was successfully used to remove a phase change which appears as an apparent change in ToF. In practice, the magnitude of the total change in ToF in rolling bearing contacts was small, 10's of nanoseconds, and all three components were significant and could not be neglected.

The technique was applied to both a model line contact formed between a moving steel roller and a flat steel plate and a roller-raceway contact in a large cylindrical roller bearing. In both cases the measured load corresponded well to the applied load. This technique shows promise for application to large bearings when both the contact dimension and the raceway deflection are large and hence lead to readily measureable ToF change.

Nomenclature

B	Bulk modulus	Pa
$(c_{zz})_0$	Ultrasonic speed in z axis in unloaded state	m/s
$(c_{zz})_P$	Ultrasonic speed in z axis in loaded state	m/s
d_0	Raceway thickness in unloaded state	m
d_P	Raceway thickness in loaded state	m
E	Young's modulus	Pa
f	Central frequency of the ultrasonic wave	Hz
K	Contact interface stiffness	Pa
l	Third order elastic constant	
l_0	Effective roller length	m
L_{zz}	Acoustoelastic constant	
N	Number of rollers in the bearing	
P	Applied load on the contact	N
ToF_0	Time of flight in unloaded state	s
ToF_P	Time of flight in loaded state	s
W	Radial load on the bearing	N
x, y, z	Coordinate axes	
δ	Surface deflection	m
Δc_{zz}	Change in speed in z axis	m/s
Δt_t	Change in time of flight caused by load	s
Δt_δ	Change in time of flight caused by raceway deflection	s
Δt_c	Change in time of flight caused by acoustoelastic effect	s
Δt_ϕ	Apparent change in time of flight caused by phase shift	s

$(\epsilon_z)_P$	Strain in z axis under applied load	
$\bar{(\epsilon_z)}_P$	Average strain through component thickness under applied load	
λ, μ	Second order elastic constant	
ν	Poisson's ratio	
ρ_0	Density in unloaded state	kg/m^3
ϕ_R	Phase of reflection coefficient	radians
ω	Angular rotation speed of roller	rad/s

Appendix

A series of experiments was performed to determine the acoustoelastic constant for a typical bearing steel. An ultrasonic transducer with centre frequency of 10 MHz was coupled directly on a bearing steel roller and longitudinal wave was passed though the roller from end to end. A strain gauge was bonded to the roller to record the actual strain. The roller was loaded in the axial direction in a hydraulic loading machine with a capacity of 250 kN. Figure 15 shows a schematic and a photograph of the apparatus. For each load case, the strain was measured using strain gauges and the ToF was recorded. The speed of ultrasound in the roller under different load was obtained from equation (2).

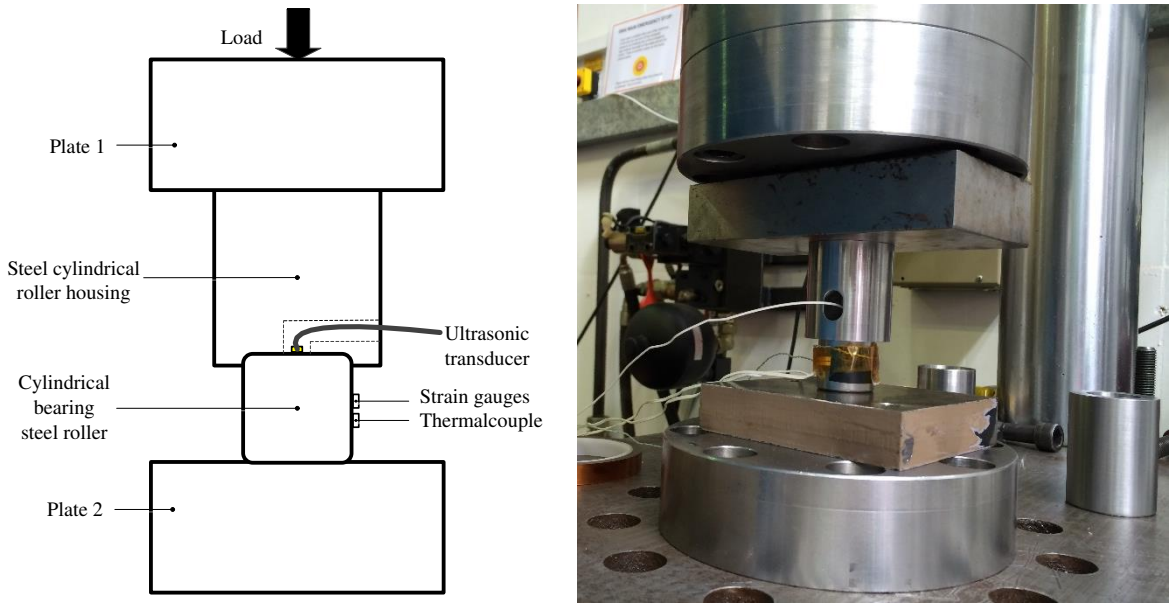

Figure 15 Schematic and photograph of the acoustoelastic constant measurement apparatus. A 10 MHz ultrasonic transducer was used to generate longitudinal wave which propagated through the roller.

Figure 16 shows the measured ultrasonic speed change plotted against the measured actual strain for three repeated load cycles. The acoustoelastic constant is obtained from the slope of

this graph using equation (18). A best fit was applied to the test data, giving the acoustoelastic constant for a typical bearing steel of -2.24. This agrees well with the acoustoelastic constant for steels measured with ultrasound by other researchers [11], who found constants varied from -2.1 to -2.45 for different steels.

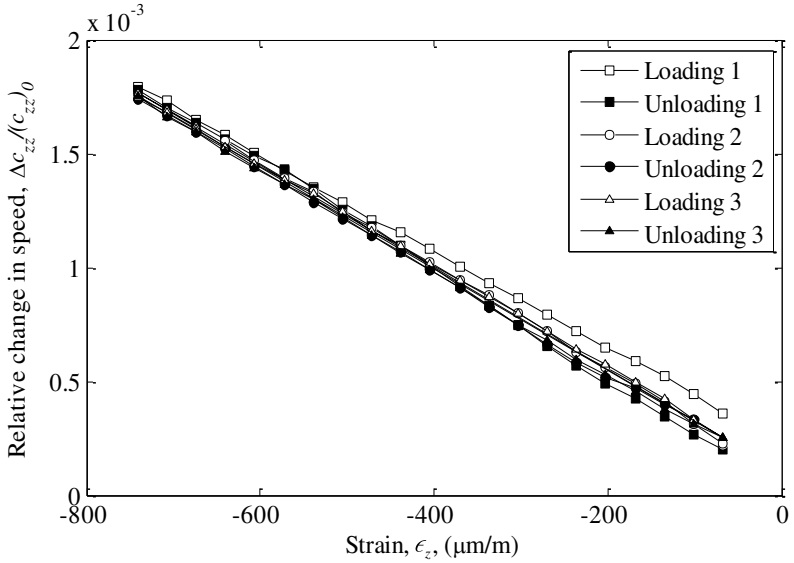

Figure 16 Measured ultrasonic speed change with strain for a bearing steel. Three loading cycles were performed. The slope of this line gives the acoustoelastic constant.

References

[1] International Organization for Standards. 2010 Rolling Bearings—Dynamic load ratings and rating life. *International standard ISO 281*.

[2] Al-Tubi I S, Long H. 2013 Prediction of wind turbine gear micropitting under variable load and speed conditions using ISO/TR 15144-1: 2010. *Proc. Inst. Mech. Engrs. Part C: J. Mech. Eng. Sci*. **227**, 1898-1914.

[3] Christopher S G, Simon J W. 2010 Physics of failure approach to wind turbine condition based maintenance. *Wind Energy* **13**, 395-405.

[4] Chen J S, Chen KW. 2005 Bearing load analysis and control of a motorized high speed spindle. *International Journal of Machine Tools and Manufacture* **45**, 1487-1493.

[5] Nässelqvist M, Gustavsson R, Aidanpää J-O. 2012 Bearing load measurement in a hydropower unit using strain gauges installed inside pivot pin. *Experimental Mechanics* **52**, 361-369.

[6] Dwyer-Joyce R S, Drinkwater B W, Quinn A M. 2001 The use of ultrasound in the investigation of rough surface interfaces. *ASME J. Tribology* **123**, 8-16.

[7] Dwyer-Joyce R S, Drinkwater B W and Donohoe C J. 2003 The measurement of lubricant-film thickness using ultrasound. *Proc. R. Soc. Lond. A* **459**, 957-976.

[8] Dwyer-Joyce R S, Harper P, Drinkwater B W. 2004 A method for the measurement of hydrodynamic oil films using ultrasonic reflection. *Tribology Letters* **17**, 337-348.

[9] Wan Ibrahim M K, Gasni D, Dwyer-Joyce R S. 2012 Profiling a ball bearing oil film with ultrasonic reflection. *Tribology Transactions* **55**, 409-421.

[10] Egle D M, Bray D E. 1976 Measurement of acoustoelastic and third-order elastic constants for rail steel. *J. Acoust. Soc. Am.* **60**, 741-744.

[11] Bray D E , Tang W. 2001 Subsurface stress evaluation in steel plates and bars using the LCR ultrasonic wave. *Nuclear Engineering and Design* **207**, 231-240.

[12] Smith R T. 1963 Stress-induced anisotropy in solids - the acousto-elastic effect. *Ultrasonics* **1,** 135-147.

[13] Tanala E, Bourse G, Fremiot M, Belleval J F. 1995 Determination of near surface residual stress on welded joints using ultrasonic methods. *NDT&E International* **28**, 83–88.

[14] Reddyhoff T, Kasolang S, Dwyer-Joyce R S, Drinkwater B W. 2005 The Phase Shift of an Ultrasonic Pulse at an Oil Layer and Determination of Film Thickness. *Proc. I. Mech. Eng.: J. of Eng. Tribol.* **219**, 387-399.

[15] Palmgren A. 1959 *Ball and Roller Bearing Engineering*, 3rd ed. California: SKF industries.

[16] Dowson D, Higginson G. 1968 Elastodynamics. *Pro. Inst. Mech. Eng.* **182**, 151-167.

[17] Wheals J C, Guern P, Dwyer-Joyce R S, Marshall M, Howard T. 2011 Ricardo Multilife bearing programme for increased reliability of offshore wind turbines. Paper presented at *European Wind Energy Conference,* Brussels, Belguim, 16 March 2011.

[18] Harris T A. 2001 *Rolling Bearing Analysis*, 4th ed. New York: John Wiley & Sons.